EPJ Web of Conferences **175**, 13021 (2018) https://doi.org/10.1051/epjconf/201817513021
Lattice 2017

Total decay and transition rates from LQCD

Maxwell T. Hansen[1,⋆], *Harvey B.* Meyer[1,2], and *Daniel* Robaina[3,⋆⋆]

[1] *Helmholtz Institut Mainz, D-55099 Mainz, Germany.*
[2] *PRISMA Cluster of Excellence and Institut für Kernphysik, Johannes Gutenberg Universität Mainz, D-55099 Mainz, Germany.*
[3] *Institut für Kernphysik, Technische Universität Darmstadt, Schlossgartenstrasse 2, D-62489 Darmstadt, Germany.*

Abstract. We present a new technique for extracting total transition rates into final states with any number of hadrons from lattice QCD. The method involves constructing a finite-volume Euclidean four-point function whose corresponding infinite-volume spectral function gives access to the decay and transition rates into all allowed final states. The inverse problem of calculating the spectral function is solved via the Backus-Gilbert method, which automatically includes a smoothing procedure. This smoothing is in fact required so that an infinite-volume limit of the spectral function exists. Using a numerical toy example we find that reasonable precision can be achieved with realistic lattice data. In addition, we discuss possible extensions of our approach and, as an example application, prospects for applying the formalism to study the onset of deep-inelastic scattering. More details are given in the published version of this work, Ref. [1].

1 Introduction

In Lattice QCD, low-energy properties of the strong force are calculated numerically in a finite, discretized spacetime box. The nonzero lattice spacing, finite volume and finite time make the system numerically solvable by means of a non-perturbative, but computationally expensive, Monte Carlo evaluation of the partition function. After a representative set of field configurations has been determiend, matrix elements of quark-field operators between finite-volume hamiltonian eigenstates can be calculated with less numerical effort.

Due to the periodic boundary conditions, usually applied in all spatial directions, the energy spectrum and the eigenstates of the finite-volume Hamiltonian cannot be the same as those of the corresponding infinite-volume theory. Nonetheless, in theories with a mass gap, like QCD, it is possible to define single-particle, finite-volume states that smoothly approach their infinite-volume counterparts. For such states, with total three-momentum projected to zero, as the box size is increased ($L \to \infty$) the pole position in the corresponding finite-volume Euclidean correlator approaches the infinite-volume value with exponentially small corrections as $E_Q(L) = M_Q + O(e^{-M_\pi L})$, where M_π is the physical mass of the lightest degree of freedom, the pion in QCD, and M_Q the mass of the particle with quantum numbers Q [2]. This exponential suppression of finite-volume artifacts, which also

⋆ Second speaker, e-mail: maxhanse@uni-mainz.de
⋆⋆ First speaker, e-mail: robaina@theorie.ikp.physik.tu-darmstadt.de

holds for matrix elements of local operators between single-particle states, can be exploited to extract masses and couplings of such states, by calculating with various values of $M_\pi L$ and extrapolating to the infinite-volume limit.

The situation is more complicated when dealing with multi-particle states, for example when studying decays into multi-hadron final states. Consider the simplest case of a finite-volume two-pion state with zero total momentum. In the case where the pions are weakly interacting, the finite-volume energy levels are given by

$$E_{2\pi}^{(n)} = 2\sqrt{M_\pi^2 + 4\pi^2 \mathbf{q}_n^2/L^2} + O(\text{interactions}/L^3)\,, \tag{1}$$

with $\mathbf{q_n} \in \mathbb{Z}^3$ a representative integer vector of the nth state, $\mathbf{q}_0^2 = 0, \mathbf{q}_1^2 = 1, \cdots$ [3]. The energy of such a state contains information about the interactions, but if we take a naive infinite-volume limit with n fixed, the energy flows to the threshold value, $2M_\pi$.

In recent years, a lot of progress has been made in accessing information about particle interactions and scattering by using the finite volume as a tool and performing a controlled extraction of the infinite-volume physics. This is based primarily on work by Lüscher [3, 4] and by Lellouch and Lüscher [5]. The original idea, developed by Lüscher, is to study two-particle scattering states in a finite volume and relate the energy spectrum to the infinite-volume two-to-two scattering amplitudes. In the past decades, Lüscher's formalism has been generalized to states with non-zero momentum in the finite volume, intrinsic spin, non-degenerate particles as well as any number of open two-particle channels [6–18]. Generalizations to three-particle scattering states are also underway [19–22].

Similarly, the Lellouch-Lüscher formalism for determining one-to-two transition amplitudes, originally in the context of $K \to \pi\pi$, has been extended to general two-hadron final states and to currents with non-zero angular-momentum, momentum and energy, enabling the extraction of semi-leptonic decay amplitudes and time-like form factors [7, 8, 16, 17, 23–27]. In Ref. [28] the Lellouch-Lüscher approach was further extended to $\mathbf{2} \longrightarrow \mathbf{2}$ transition amplitudes induced by an external probe, providing a rigorous path towards resonance form factors. Also Ref. [29] used techniques based in the Lellouch-Lüscher approach to analyze long-distance contributions to K_L-K_S mixing from a finite-volume Euclidean four-point function. Going beyond these types of approaches, many authors have considered various methods for extracting transition and scattering amplitudes and rates by analyzing the properties of lattice two- and four-point functions [30–37]. In the published version, Ref. [1], we review various contributions and compare and contrast these to our own method.

As the final-state energy is increased, and more channels, with more particles per channel, open up, formalisms based on the paradigm of Lellouch and Lüscher, and its numerical implementation, become increasingly challenging. Here we propose a new approach to calculate total decay widths and transition rates for QCD-stable particles into final states with any number of hadrons. Our method involves the calculation of a Euclidean four-point function and the extraction of its associated spectral function. The inverse problem of accessing the spectral function is solved by means of the Backus-Gilbert method [38–41]. This is a linear method which is exact in the sense that it converges to the correct solution in the limit of infinite data with vanishing uncertainty. The model-independent estimator also provides a smoothing that is required for a well-defined infinite-volume limit.

In the following two sections we introduce the formalism and provide a numerical test case. In Sec. 4 we give a detailed comparison the Lellouch-Lüscher approach, followed by a discussion of various extensions in Sec. 5 and applications in Sec. 6.

2 Formalism and methodology

In this section we highlight the key equations and relations needed in our method for estimating total decay and transition rates from lattice QCD. For a more detailed and complete derivation we refer to the original publication, Ref. [1].

2.1 Infinite-volume discussion

Consider a QCD-stable state $|D, \mathbf{P}\rangle$ with energy E_D, representing, for example, a D-meson with 3-momentum $\mathbf{P}$. Now imagine a small perturbation $\mathcal{H}_Q$ that allows it to decay (for example a weak hamiltonian density). At leading order in the weak interaction, the total decay width of the D-meson into all multiparticle states with quantum numbers Q is given by

$$\Gamma_{D\to Q} \equiv \frac{1}{2M_D}\sum_{\alpha}\frac{1}{S_\alpha}\int d\Phi_\alpha(k_1,\cdots,k_{N_\alpha})|\langle E_D,\mathbf{P},\alpha;\text{out}|\mathcal{H}_Q(0)|D,\mathbf{P}\rangle|^2\,, \tag{2}$$

$$= \frac{1}{2M_D}\int d^4x\,\langle D,\mathbf{P}|\mathcal{H}_Q(x)\mathcal{H}_Q(0)|D,\mathbf{P}\rangle\,, \tag{3}$$

where we have eliminated the explicit dependence on the final states in the second line. The sum over α labels the different multi-particle states, $d\Phi_\alpha(k_1,\cdots,k_{N_\alpha})$ represents the standard Lorentz-invariant phase-space measure for an N_α-particle state and S_α its corresponding symmetry factor.

Both versions of the above formula will be important throughout this work and can be derived from a more general object that we call the *transition spectral function*

$$\rho_{Q,\mathbf{P}}(E,\mathbf{p}) \equiv \frac{1}{n_\lambda}\sum_{\lambda,\alpha}\frac{1}{S_\alpha}\int d\Phi_\alpha(k_1,\cdots,k_{N_\alpha})|\langle E,\mathbf{p},\alpha;\text{out}|\mathcal{J}_Q(0)|N,\mathbf{P},\lambda\rangle|^2\,. \tag{4}$$

In order to extend the validity of our approach, here we have replaced the D-meson state with a nucleon $|N,\mathbf{P},\lambda\rangle$ with azimuthal spin component λ and momentum $\mathbf{P}$. We have also included a spin average, i.e. this expression is appropriate for an unpolarized initial state. The small perturbation $\mathcal{H}_Q$ has been replaced by a generic local current, $\mathcal{J}_Q$ (e.g. the electromagnetic current for considering deep-inelastic scattering processes) that can change the total energy and momentum of the system by an amount $q \equiv p - P$.

Using the completeness of the QCD outstates we find

$$\rho_{Q,\mathbf{P}}(E,\mathbf{p}) = \frac{1}{n_\lambda}\sum_{\lambda}\int d^4x\, e^{i(E-E_N)t - i(\mathbf{p}-\mathbf{P})\cdot\mathbf{x}}\,\langle N,\mathbf{P},\lambda|\mathcal{J}_Q^\dagger(x)\mathcal{J}_Q(0)|N,\mathbf{P},\lambda\rangle\,. \tag{5}$$

Note that this is consistent with Eq. (2) as can be seen by setting $p = P$ and replacing the nucleon with the D-meson

$$\Gamma_{D\to Q} = \frac{1}{2M_D}\rho_{Q,\mathbf{P}}(E_D,\mathbf{P})\,. \tag{6}$$

Thus, the transition spectral function can be written as the expectation value of a product of field operators in a one-particle external state. We stress that, in this subsection, all matrix elements are evaluated in infinite volume and with real Minkowski time coordinates.

2.2 Finite-volume lattice approach

Let us now consider the most closely related Euclidean correlator we can calculate on the lattice

$$G_{Q,\mathbf{P}}(\tau,\mathbf{x},L) \equiv 2E_N L^6 e^{-E_N\tau+i\mathbf{P}\cdot\mathbf{x}} \lim_{\tau_f\to\infty}\lim_{\tau_i\to-\infty} \frac{\sum_\lambda \langle \Psi_\lambda(\tau_f,\mathbf{P})\mathcal{J}_Q^\dagger(\tau,\mathbf{x})\mathcal{J}_Q(0)\Psi_\lambda^\dagger(\tau_i,\mathbf{P})\rangle_{\text{conn}}}{\sum_\lambda \langle \Psi_\lambda(\tau_f,\mathbf{P})\Psi_\lambda^\dagger(\tau_i,\mathbf{P})\rangle}\,, \tag{7}$$

where $\Psi_\lambda^\dagger(\tau_i,\mathbf{P})$ is an interpolator for the nucleon (or any other QCD-stable state) with total momentum $\mathbf{P}$ and spin component λ, and the subscript "conn" indicates subtraction of $\langle\mathcal{J}_Q^\dagger(\tau,\mathbf{x})\mathcal{J}_Q(0)\rangle\langle\Psi_\lambda(\tau_f,\mathbf{P})\Psi_\lambda^\dagger(\tau_i,\mathbf{P})\rangle$. Throughout this work we take $\tau > 0$.

Evaluating the large time limits, inserting a complete set of finite-volume states and projecting to definite momentum $\mathbf{p}$ we find

$$\begin{aligned}\widetilde{G}_{Q,\mathbf{P}}(\tau,\mathbf{p},L) &\equiv \int d^3\mathbf{x}\, e^{-i\mathbf{p}\cdot\mathbf{x}} G_{Q,\mathbf{P}}(\tau,\mathbf{x},L)\,,\\ &= 2E_N L^6 \sum_k e^{-E_k(L)\tau}|M_{k,N\to Q}(\mathbf{p},L)|^2\,,\end{aligned} \tag{8}$$

where $M_{k,N\to Q}(\mathbf{p},L) \equiv \frac{1}{n_\lambda}\sum_\lambda \langle E_k(L),\mathbf{p},Q|\mathcal{J}_Q(0)|N,\mathbf{P},\lambda\rangle_L$ are spin-averaged matrix elements evaluated between a finite-volume multi-particle state and a single-particle external state.

Equation (8) can be rewritten as

$$\widetilde{G}_{Q,\mathbf{P}}(\tau,\mathbf{p},L) = \int_0^\infty \frac{d\omega}{2\pi}\, e^{-\omega\tau}\rho_{Q,\mathbf{P}}(\omega,\mathbf{p},L)\,, \tag{9}$$

where

$$\rho_{Q,\mathbf{P}}(E,\mathbf{p},L) \equiv 2E_N\, L^6 \sum_k |M_{k,N\to Q}(\mathbf{p},L)|^2\; 2\pi\,\delta(E-E_k(L))\,, \tag{10}$$

is the finite-volume spectral function. Substituting this sum of delta functions into Eq. (9) and evaluating the integral immediately gives back Eq. (8). We emphasize at this stage that, while the infinite-volume spectral function gives direct access to the decay width, in the finite volume we have a sum of delta peaks. Naively sampling $\rho_{Q,\mathbf{P}}(E,\mathbf{p},L)$ at a specific energy cannot give any useful information.

In order to recover the total decay width, we need to construct a sensible infinite-volume limit of the spectral function. To do so we introduce $\widehat{\delta}_\Delta(\overline{\omega},\omega)$ as a regularized delta function, centered at $\overline{\omega}$ with characteristic width Δ. We require only that this satisfies

$$\int_0^\infty d\omega\,\widehat{\delta}_\Delta(\overline{\omega},\omega) = 1, \qquad \lim_{\Delta\to0}\int_0^\infty d\omega\,\widehat{\delta}_\Delta(\overline{\omega},\omega)\phi(\omega) = \phi(\overline{\omega})\,, \tag{11}$$

for a smooth test function $\phi(\omega)$. In our approach, $\widehat{\delta}_\Delta(\overline{\omega},\omega)$ will tend to zero exponentially for large ω.

We then define

$$\widehat{\rho}_{Q,\mathbf{P}}(\overline{\omega},\mathbf{p},L,\Delta) \equiv \int_0^\infty d\omega\,\widehat{\delta}_\Delta(\overline{\omega},\omega)\,\rho_{Q,\mathbf{P}}(\omega,\mathbf{p},L)\,. \tag{12}$$

This replaces the sum over delta functions with a smooth function that has a well-defined infinite-volume limit. Thus it follows that differential transition rates, as well as total decay rates, can be accessed from the lattice framework via the limits

$$\rho_{Q,\mathbf{P}}(E,\mathbf{p}) = \lim_{\Delta\to0}\lim_{L\to\infty}\widehat{\rho}_{Q,\mathbf{P}}(E,\mathbf{p},L,\Delta)\,, \tag{13}$$

where the order of limits is crucial.

The Backus-Gilbert method applied to the inverse problem of determining $\rho_{Q,\mathbf{P}}(E,\mathbf{p},L)$ from $\widetilde{G}_{Q,\mathbf{P}}(\tau,\mathbf{p},L)$ leads precisely to smoothed quantities of the form given in Eq. (12). If the correlation function is known at a discrete set of Euclidean times, τ_j, then the 'resolution function' $\widehat{\delta}_\Delta(\overline{\omega},\omega)$ should be constructed from the Laplace kernel,

$$\widehat{\delta}_\Delta(\overline{\omega},\omega) = \sum_j C_j(\overline{\omega},\Delta)\, e^{-\omega\tau_j}, \tag{14}$$

with coefficients C_j chosen so as to minimize the width

$$\Delta = \int_0^\infty d\omega\, (\overline{\omega}-\omega)^2\, \widehat{\delta}_\Delta(\overline{\omega},\omega)^2\,, \tag{15}$$

under the unit-area constraint of Eq. (11). The Backus-Gilbert method then yields an estimate of the smoothed spectral function

$$\widehat{\rho}_{Q,\mathbf{P}}(\overline{\omega},\mathbf{p},L,\Delta) = 2\pi \sum_j C_j(\overline{\omega},\Delta)\, \widetilde{G}_{Q,\mathbf{P}}(\tau_j,\mathbf{p},L)\,. \tag{16}$$

Of course, given the limitations of a realistic set-up, it is not possible to evaluate the ordered limit given in Eq. (13). Instead, our idea is to search for a window in the (Δ, L) plane which gives a good numerical estimate of the target. Heuristically, the volume needs to be large enough that the density of intermediate finite-volume levels in a given ω-range is comparable to $1/\Delta$. In this way, the smoothing procedure will not resolve individual peak structures coming from finite-volume states. In the following section we perform a numerical test to show how this might be done.

3 Numerical test case

This section is devoted to illustrating, by means of a numerical example, to what extent our procedure is able to reproduce infinite-volume total decay widths.

3.1 Basic set-up

The input data consists of a Euclidean correlation function $\widetilde{G}_{Q,\mathbf{0}}(\tau_i,\mathbf{0},L)$ of the type presented in Eq. (7), evaluated at N_τ discrete Euclidean time slices up to a maximum extent L, at which point we assume that the signal is lost. In this example we ignore finite-temperature effects, i.e. we take the Euclidean temporal direction to have infinite extent.

We study a toy theory with three scalar particles denoted by, π, K and ϕ, with physical masses M_π, M_K, M_ϕ, respectively, and interactions given by

$$\mathcal{L}(x) \supset \frac{\lambda}{6}\phi(x)\pi(x)^3 + \frac{gM_\phi}{2}\phi(x)K(x)^2\,, \qquad 3M_\pi < 2M_K < M_\phi\,. \tag{17}$$

Treating the interactions perturbatively, our goal is extract the spectral function $\rho_{Q,\mathbf{0}}(\omega,\mathbf{0})$ from the corresponding finite-volume Euclidean correlator, and compare this to the result of a direct infinite-volume calculation. When evaluated at $\omega = M_\phi$, this spectral function then gives the total decay width of the ϕ particle to leading order in the dimensionless couplings λ and g. We stress that this is only a toy set-up and bears no relation (other than superficial kinematic similarity) to the physical particles that carry these names.

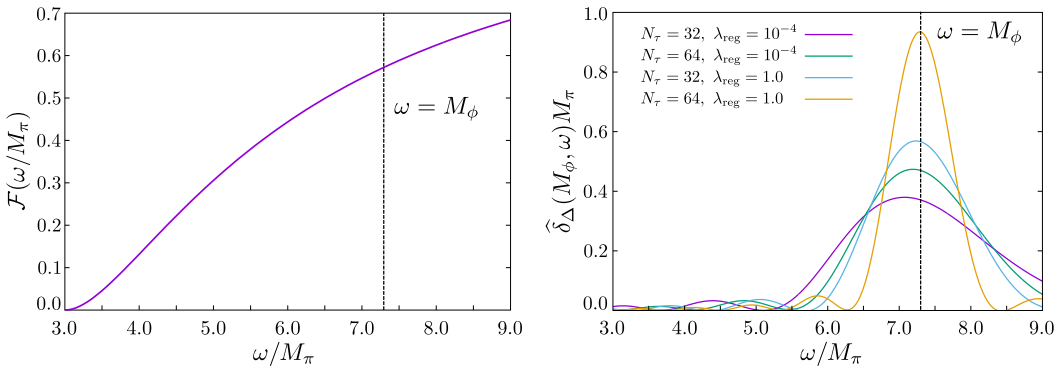

Figure 1. Left: The function $\mathcal{F}(\omega/M_\pi)$ gives the three-body phase space with respect to the massless case. The function interpolates from 0 at three-particle threshold [$\mathcal{F}(3) = 0$] to unity at infinite ω [$\lim_{\omega\to\infty}\mathcal{F}(\omega/M_\pi) = 1$]. Right: Various resolution functions, plotted as a function of ω with $\overline{\omega} = M_\phi$. The resolution functions with $\lambda_{\rm reg} = 10^{-4}$ were used in the analysis. The unregulated curves, with $\lambda_{\rm reg} = 1.0$, show how the Backus-Gilbert method converges to sharply peaked resolution functions as N_τ is increased.

Before turning to the inverse problem of calculating $\widehat{\rho}_{\phi\to Q,\mathbf{0}}(\overline{\omega},\mathbf{0},L,\Delta)$, we need to construct the finite-volume Euclidean correlator that will serve as input data. Following Eq. (8)

$$\widetilde{G}_{\phi\to Q,\mathbf{0}}(\tau,\mathbf{0},L) = 2M_\phi L^6\left(\sum_k e^{-E_k(L)\tau}|M_{k,\phi\to KK}(\mathbf{0},L)|^2 + \sum_{k'} e^{-E_{k'}(L)\tau}|M_{k',\phi\to\pi\pi\pi}(\mathbf{0},L)|^2\right), \tag{18}$$

where the indices k and k' label two- and three-particle finite-volume states respectively. The full correlator that serves as input for the Backus-Gilbert procedure is then

$$\widetilde{G}_{\phi\to Q,\mathbf{0}}(\tau_i,\mathbf{0},L) = \frac{1}{M_\pi^3}\widetilde{G}_{KK}(\tau_i,\mathbf{0},L) + \frac{1}{M_\pi^3}\widetilde{G}_{\pi\pi\pi}(\tau_i,\mathbf{0},L)\,, \tag{19}$$

where we have used M_π to make the input data dimensionless. Finally, since we want to reconstruct the full spectral function and compare to the $L\to\infty$ result, we directly calculate the latter

$$\frac{1}{2M_\phi M_\pi}\rho_{\phi\to Q,\mathbf{0}}(\omega,\mathbf{0}) = \frac{\lambda^2}{3072\pi^3}\frac{M_\pi}{M_\phi}\left(\frac{\omega}{M_\pi}\right)^2\mathcal{F}(\omega/M_\pi)\theta(\omega-3M_\pi) + \frac{g^2}{32\pi}\frac{M_\phi}{M_\pi}\sqrt{1-\frac{4M_K^2}{\omega^2}}\theta(\omega-2M_K)\,. \tag{20}$$

Here $\mathcal{F}(M_\phi/M_\pi)$, shown in the left pannel of Fig. 1, measures the reduction of phase space relative to the case of $M_\pi = 0$ where the decay products are massless. Note in particular that $\mathcal{F}(3) = 0$ and $\mathcal{F}(\infty) = 1$. This function has no simple analytic form, but can easily be calculated numerically to arbitrary precision. Its exact definition is given in the original publication, Ref. [1], where we also provide a detailed derivation of the matrix elements needed for this analysis in finite as well as infinite volume.

3.2 Inverse problem and smoothing via Backus-Gilbert

The aim is to recover the full spectral function

$$\rho_{\phi\to Q,\mathbf{0}}(\overline{\omega},\mathbf{0}) = \lim_{\Delta\to 0}\lim_{L\to\infty}\widehat{\rho}_{\phi\to Q,\mathbf{0}}(\overline{\omega},\mathbf{0},L,\Delta)\,, \tag{21}$$

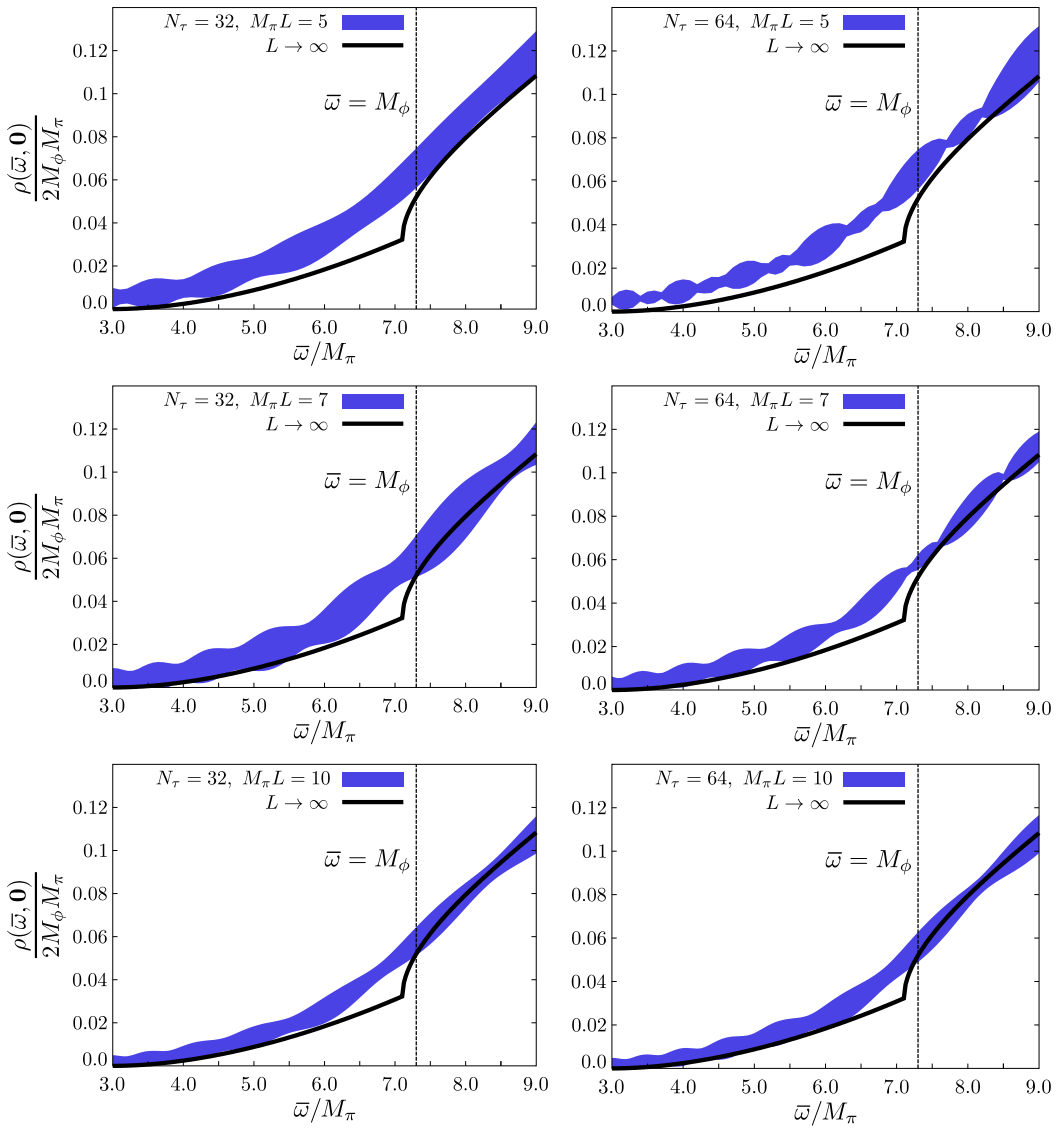

Figure 2. Output of the regulated Backus-Gilbert algorithm for different values of $M_\pi L = 5, 7, 10$ and $N_\tau = 32, 64$. The ratios of $M_\phi/M_\pi, M_K/M_\pi$ and the coupling constants are given in the text.

where in particular for $\overline{\omega} = M_\phi$ we get an estimate for the total decay width

$$\frac{1}{2M_\phi M_\pi} \lim_{\Delta \to 0} \lim_{L \to \infty} \widehat{\rho}_{\phi \to Q,\mathbf{0}}(M_\phi, \mathbf{0}, L, \Delta) = \frac{\Gamma_{\phi \to KK}}{M_\pi} + \frac{\Gamma_{\phi \to \pi\pi\pi}}{M_\pi} \,. \tag{22}$$

For the numerical application, we choose $M_K/M_\pi = 3.55$ and $M_\phi/M_\pi = 7.30$, $g = 1$ and $\lambda = 10\sqrt{8}$. We use as input points $\tau_i = i \cdot a$, with $aM_\pi = 0.066$ and $1 \le i \le N_\tau$. As explained in

Sec. 2.2, we construct a family of resolution functions $\widehat{\delta}_\Delta(\overline{\omega},\omega)$ by finding the optimal coefficients $C_i(\overline{\omega},\Delta)$, $(i = 1,\ldots,N_\tau)$, that minimize the width subject to the area constraint of Eq. (11). The width is controlled by the number of points, as can be seen from Fig. 1, where we give examples of resolution functions used in the analysis, centered at $\omega = M_\phi$. The corresponding estimator $\widehat{\rho}_{\mathcal{Q},\mathbf{0}}(\overline{\omega},\mathbf{0})$ is calculated via Eq. (16). The results for various sets of parameters are shown in Fig. 2.

Since Backus-Gilbert is a linear method, an error estimate on $\widehat{\rho}_{\mathcal{Q},\mathbf{0}}(\overline{\omega},\mathbf{0})$ has to come through the covariance matrix of the input data $\widetilde{G}_Q(\tau_i,\mathbf{0},L)$. We take a realistic covariance matrix, S_{ij}, from a pseudoscalar meson two-point function calculated on an $N_f = 2$ CLS ensemble, that we have used in the past in a similar context. (See Appendix C of Ref. [41].) We scale the covariance matrix to give the same relative uncertainty (about 2%) on the toy correlator, $\widetilde{G}_Q(\tau_i,\mathbf{0},L)$, as was observed on the actual lattice data.

In order to determine the optimal coefficients, $C_i(\overline{\omega},\Delta)$, a poorly conditioned matrix $W_{ij}(\overline{\omega}) \equiv \int_0^\infty d\omega e^{-\omega\tau_i}(\omega-\overline{\omega})^2 e^{-\omega\tau_j}$ must be inverted (ideally with high precision). The error on $\widehat{\rho}_{\mathcal{Q},\mathbf{0}}(\overline{\omega},\mathbf{0})$ is kept under control by making the replacement $W_{ij}(\overline{\omega}) \to \lambda_{\text{reg}} W_{ij}(\overline{\omega}) + (1-\lambda_{\text{reg}})S_{ij}$. In this way the magnitudes of the coefficients $C_i(\overline{\omega},\Delta)$, which otherwise exhibit large oscillations as a function of i, are tamed, and the statistical error on $\widehat{\rho}_{\mathcal{Q},\mathbf{0}}(\overline{\omega},\mathbf{0})$ can be kept under control. In the present example, we aim for a precision of $5-10\%$ and find that this is achieved with $\lambda_{\text{reg}} \sim 10^{-4}$. The regulation parameter, λ_{reg}, parametrizes a trade-off between resolving power (smaller Δ) and statistical error. For a more detailed explanation on the choice of λ_{reg} see the discussion in Sec. IV E of Ref. [41].

4 Comparison to the Lellouch-Lüscher formalism

The mostly widely used approach for extracting decay and transition observables into multi-hadron final states is the formalism of Lellouch and Lüscher together with its many extensions [5, 7, 8, 16, 17, 23–27]. We focus here on the original Lellouch-Lüscher result for extracting the decay amplitude for $K \to \pi\pi$ from a corresponding finite-volume matrix element. We define the finite-volume matrix element

$$M_{k,K\to\pi\pi}(L) \equiv \langle k,L|\mathcal{H}(0)|K,L\rangle\,, \tag{23}$$

where both finite-volume states have unit normalization and zero three-momentum. $\mathcal{H}(0)$ is a weak hamiltonian density and $\langle k,L|$ is the kth excited state with the quantum numbers of two pions. The Lellouch-Lüscher formalism then gives the relation of this matrix element to the infinite-volume decay amplitude

$$A_{K\to\pi\pi}[E_k(L)] \equiv \langle E_k(L),\pi\pi,\text{out}|\mathcal{H}(0)|K\rangle\,, \tag{24}$$

where the infinite-volume states have standard relativistic normalization.

The relation takes the form of a proportionality factor

$$|M_{k,K\to\pi\pi}(L)|^2 = \frac{C_k}{4M_K E_k(L)^2 L^9}\left|A_{K\to\pi\pi}[E_k(L)]\right|^2, \tag{25}$$

where

$$C_k \equiv \left(\frac{1}{4\pi^2 q^2}\frac{\partial\phi(q)}{\partial q} + \frac{2\pi}{p^2L^3}\frac{\partial\delta_{\pi\pi}(p)}{\partial p}\right)^{-1}_{q=Lp/(2\pi),\ \ p=\sqrt{E_k(L)^2/4-M_\pi^2}}. \tag{26}$$

Here $\phi(q)$ is a known function and $\delta_{\pi\pi}(p)$ is the s-wave $\pi\pi \to \pi\pi$ scattering phase shift due to the strong force only. The relation is valid up to neglected corrections scaling as $e^{-M_\pi L}$. Strictly speaking, this relation only gives the kaon decay amplitude when the volume is tuned such that $E_k(L) = M_K$. However, the result holds away form this tuning as was shown in subsequent work.

To illustrate the connection between the Lellouch-Lüscher approach and the method described here, we first show the consistency of the two. In particulate we note that, in the case where the initial hadron is a kaon and the current a weak hamiltonian mediating $K \to \pi\pi$, then the smeared spectral function defined in Eq. (12) above can be written

$$\widehat{\rho}_{Q,\mathbf{0}}(E,\mathbf{0},L,\Delta) \equiv \sum_k \frac{C_k}{2E_k(L)^2L^3}\left|A_{K\to\pi\pi}[E_k(L)]\right|^2 2\pi\widehat{\delta}_\Delta(E,E_k(L))\,, \tag{27}$$

where we have substituted the relation between finite- and infinite-volume matrix elements to express the right-hand side in terms of the transition amplitude $A_{K\to\pi\pi}$.

With this expression in hand we can formally take the infinite-volume limit

$$\lim_{L\to\infty}\widehat{\rho}_{Q,\mathbf{0}}(E,\mathbf{0},L,\Delta) = \lim_{L\to\infty}\sum_k \frac{\nu_k}{2(2\omega_\mathbf{k})^2L^3}\left|A_{K\to\pi\pi}[2\omega_\mathbf{k}]\right|^2 2\pi\widehat{\delta}_\Delta(E,2\omega_\mathbf{k})\,, \tag{28}$$

$$= \lim_{L\to\infty}\frac{1}{2}\frac{1}{L^3}\sum_\mathbf{k}\frac{1}{(2\omega_\mathbf{k})^2}\left|A_{K\to\pi\pi}[2\omega_\mathbf{k}]\right|^2 2\pi\widehat{\delta}_\Delta(E,2\omega_\mathbf{k})\,, \tag{29}$$

$$= \frac{1}{2}\int\frac{d^3\mathbf{k}}{(2\pi)^3(2\omega_\mathbf{k})^2}\left|A_{K\to\pi\pi}[2\omega_\mathbf{k}]\right|^2 2\pi\widehat{\delta}_\Delta(E,2\omega_\mathbf{k})\,. \tag{30}$$

In the first line we have used the identity $\lim_{L\to\infty} C_k = \nu_k$ where ν_k is defined to count the degeneracy of non-interacting, non-indentical two-particle states, i.e. $\nu_0 = 1, \nu_1 = 6, \cdots$. We have also replaced $E_k(L) \to 2\omega_\mathbf{k}$ in the first line. This is justified by the observation that the gap between interacting and non-interacting states vanishes in the infinite-volume limit.[1] In the second line we have used $\sum_k \nu_k f(2\omega_\mathbf{k}) = \sum_\mathbf{k} f(2\omega_\mathbf{k})$ for any smooth function $f(2\omega_\mathbf{k})$ and in the third line we have used the infinite-volume limit to replace the momentum sum over the smooth function with an integral.

Equation (30) is nearly the definition of a total decay rate, differing only due to the fact that E is treated as a free parameter and because $\widehat{\delta}$ is a smeared resolution function with nonzero width. Both of these differences are removed in the final step, embodied in Eqs. (6) and (13). This leads to

$$\Gamma_{K\to\pi\pi} = \frac{1}{2M_K}\lim_{\Delta\to 0}\lim_{L\to\infty}\widehat{\rho}_{Q,\mathbf{0}}(M_K,\mathbf{0},L,\Delta) = \frac{1}{4M_K}\int\frac{d^3\mathbf{k}}{(2\pi)^3M_K^2}\left|A_{K\to\pi\pi}[M_K]\right|^2 2\pi\delta(M_K-2\omega_\mathbf{k})\,, \tag{31}$$

which is the standard relation between amplitude and rate for decay into two identical scalars.

Having illustrated the consistency between the Lellouch-Lüscher relation and the Backus-Gilbert spectral function approach, we close this section by comparing the two methods. The key advantages of the Lellouch-Lüscher formalism are that it allows one to access amplitudes rather than rates, it allows one to pick out a particular asymptotic out-state, i.e. to study exclusive processes, and it circumvents the need for an infinite-volume limit by explicitly incorporating the finite-volume effects into the formalism. By contrast, the advantages of the Backus-Gilbert approach are that it works for any number of particles and any number of open channels, does not require identifying individual energy levels, and is indeed expected to work better when the density of states is high, implying a denser coverage of the spectral function. In Table 1 we give a more thorough comparison.

5 Extensions and modifications

In this section we consider various extensions and modifications of our approach for using the Backus-Gilbert method to estimate infinite-volume spectral functions.

[1] This statement is somewhat subtle as additional finite-volume states can arise, for example due to resonances, with no non-interacting counterpart. However, these individual states have vanishing measure as $L \to \infty$ and cannot spoil the limit.

	Lellouch-Lüscher	Backus-Gilbert spectral function
Physical observable	transition and decay amplitudes (specific out states)	total transition and decay rates (specific QCD quantum numbers)
Status of the formalism	accomodates all types of two-particle channels (three-particle underway)	accomodates all possible multi-particle channels
Potential sources of uncertainty/challenges	– neglected open channels (higher partial waves) – estimating S-matrix derivatives – relating different energies	– signal for $G(\tau)$ – Backus-Gilbert inversion – estimating double limit
Best when...	– few open channels – many finite-volume constraints – low density of states	– many open channels – many particles per channel – high density of states – slowly varying spectral function

Table 1. Comparison of the Lellouch-Lüscher and Backus-Gilbert approaches. In potential uncertainties of Lellouch-Lüscher, 'relating different energies' refers to the practical difficulty of determining multiple constraints at the same center-of-mass energy for coupled-channel scattering and decay amplitudes.

5.1 Adjusting the starting threshold

To explain our first modification, we return to the spectral decomposition given in Eq. (8) and rewrite this as

$$\widetilde{G}_{\mathcal{Q},\mathbf{P}}(\tau,\mathbf{p},L) = 2E_N L^6 \sum_{k,E_k<E_{\text{th}}} e^{-E_k(L)\tau} |M_{k,N\to\mathcal{Q}}(\mathbf{p},L)|^2 + \widetilde{G}^{E>E_{\text{th}}}_{\mathcal{Q},\mathbf{P}}(\tau,\mathbf{p},L)\,, \tag{32}$$

with

$$\widetilde{G}^{E>E_{\text{th}}}_{\mathcal{Q},\mathbf{P}}(\tau,\mathbf{p},L) \equiv 2E_N L^6 \sum_{k,E_k>E_{\text{th}}} e^{-E_k(L)\tau} |M_{k,N\to\mathcal{Q}}(\mathbf{p},L)|^2\,. \tag{33}$$

Here we have simply separated the sum over states into two sets, with energies above and below a given threshold, denoted E_{th}.

Note that, if we choose E_{th} to be the lowest lying threshold with more than two particles, then all of the states satisfying $E_k < E_{\text{th}}$ can be treated with the Lellouch-Lüscher formalism and extensions. In particular, the individual transition amplitudes—and from this the total transition rate—can be determined by measuring the finite-volume energies and matrix elements, and applying the formalism sketched above.

With the two-particle matrix elements and energies in hand, one can next determine $\widetilde{G}^{E>E_{\text{th}}}$ by measuring the full correlation function and then subtracting the known contributions from two-particle states. The advantage is that this subtracted correlator satisfies a modified inverse-problem of the form

$$\widetilde{G}^{E>E_{\text{th}}}_{\mathcal{Q},\mathbf{P}}(\tau,\mathbf{p},L) = \int_{E_{\text{th}}}^{\infty} \frac{d\omega}{2\pi}\, e^{-\omega\tau} \rho_{\mathcal{Q},\mathbf{P}}(\omega,\mathbf{p},L)\,, \tag{34}$$

where the integration over ω starts at a higher threshold.

For example, in the case of a $\pi\pi$ system, this approach could be applied with $E_{\text{th}} = 4M_\pi$. In this case the Backus-Gilbert resolution function would first be defined for $\overline{\omega} > 4M_\pi$ and would be most

narrow around this value. This should allow one to push to higher values of $\overline{\omega}$ before the resolution function degrades. In addition, applying the Backus-Gilbert inversion from this higher threshold may lead to reduced finite-volume effects, since the density of two- and four-pion finite-volume states above $4M_\pi$ is larger than that of two-pion states in isolation below the threshold.

5.2 Modifying the Backus-Gilbert kernel

A second possible modification of the Backus-Gilbert method is to adjust the inversion kernel in order to reduce the effect of the smearing. To explain this, we suppose some ansatz for the infinite-volume spectral function, $\rho^{\text{Ansatz}}_{\mathcal{Q},\mathbf{P}}(\omega, \mathbf{p})$. Then the Laplace inverse problem, Eq. (9), can be trivially rewritten as

$$\widetilde{G}_{\mathcal{Q},\mathbf{P}}(\tau, \mathbf{p}, L) = \int_0^\infty \frac{d\omega}{2\pi} \left[\rho^{\text{Ansatz}}_{\mathcal{Q},\mathbf{P}}(\omega, \mathbf{p})\, e^{-\omega\tau}\right] \left[\frac{\rho_{\mathcal{Q},\mathbf{P}}(\omega, \mathbf{p}, L)}{\rho^{\text{Ansatz}}_{\mathcal{Q},\mathbf{P}}(\omega, \mathbf{p})}\right], \tag{35}$$

where we have simply multiplied and divided by $\rho^{\text{Ansatz}}_{\mathcal{Q},\mathbf{P}}$ in the integrand.

The non-trivial step is to apply the Backus-Gilbert algorithm using $\rho^{\text{Ansatz}}_{\mathcal{Q},\mathbf{P}}(\omega, \mathbf{p})e^{-\omega\tau}$ rather than just $e^{-\omega\tau}$ as the input kernel. That is, one determines the coefficients by minimizing the width of a new resolution function

$$\widehat{\delta}_\Delta(\overline{\omega}, \omega) = \sum_j C_j(\overline{\omega}, \Delta)\, \rho^{\text{Ansatz}}_{\mathcal{Q},\mathbf{P}}(\omega, \mathbf{p})\, e^{-\omega\tau_j}\,. \tag{36}$$

The result of this modified approach is an alternative smearing of the spectral function, given by

$$\widehat{\rho}'_{\mathcal{Q},\mathbf{P}}(\overline{\omega}, \mathbf{p}, L, \Delta) = 2\pi\rho^{\text{Ansatz}}_{\mathcal{Q},\mathbf{P}}(\overline{\omega}, \mathbf{p}) \sum_j C_j(\overline{\omega}, \Delta)\, \widetilde{G}_{\mathcal{Q},\mathbf{P}}(\tau_j, \mathbf{p}, L)\,, \tag{37}$$

$$= \rho^{\text{Ansatz}}_{\mathcal{Q},\mathbf{P}}(\overline{\omega}, \mathbf{p}) \int d\omega\, \widehat{\delta}_\Delta(\overline{\omega}, \omega)\, \frac{\rho_{\mathcal{Q},\mathbf{P}}(\omega, \mathbf{p}, L)}{\rho^{\text{Ansatz}}_{\mathcal{Q},\mathbf{P}}(\omega, \mathbf{p})}\,. \tag{38}$$

We stress that, regardless of the value of $\rho^{\text{Ansatz}}_{\mathcal{Q},\mathbf{P}}$, the altered spectral function, $\widehat{\rho}'$, is guaranteed to approach the unique infinite-volume, unsmeared result when the ordered double limit of Eq. (13) is taken. Thus, the alternative approach represents a modification of the combined finite-volume and smearing effects, and a well chosen $\rho^{\text{Ansatz}}_{\mathcal{Q},\mathbf{P}}$ could well minimize the deviations from the target quantity. In particular we note that the smearing in Fig. 2 is particularly noticeable near the two-particle cusp. Building this cusp into the ansatz would likely reduce the discrepancy. The locations of the cusps are of course known on any given lattice from single-particle spectroscopy, so that incorporating these seems feasible.

5.3 Suppressing finite-volume effects

The final extension that we wish to outline here is an idea to reduce the finite-volume effects by identifying certain values of $\overline{\omega}$ for which they are suppressed; some remarks along these lines were made in Ref. [42], Sec. (3.8). To explain this we consider the spectral function of a non-interacting theory, at energies where only a single two-scalar state can go on shell. Taking the matrix element coupling the initial hadron to the final two-particle state to be constant, we find that the smeared, finite-volume spectral function takes the form

$$\widehat{\rho}_{\text{free}}(\overline{\omega}, L, \Delta) \equiv \int_0^\infty d\omega \left[\frac{1}{L^3}\sum_{\mathbf{k}} \frac{\delta(\omega - 2\omega_{\mathbf{k}})}{4\omega_{\mathbf{k}}^2}\right] \frac{e^{-(\overline{\omega}-\omega)^2/(2\Delta^2)}}{\sqrt{2\pi}\Delta}\,. \tag{39}$$

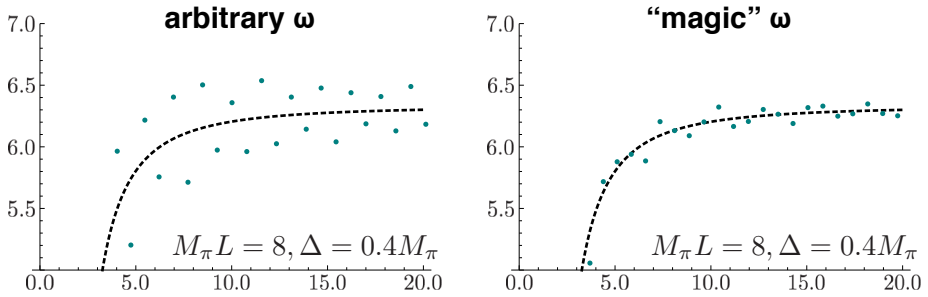

Figure 3. A comparison of generic ω values (left points) with the special values described in the text (right points). The "magic" values have smaller finite-volume effects on average and therefore lie closer to the target function, shown by the dashed black line. This example was generated using the free spectral function defined in Eq. (39).

Here we have dropped the overall constant parametrizing the coupling of initial and final states. We have also taken the resolution functions to be Gaussian. At low energies, this tends to be a good approximation for the resolution functions achieved by the Backus-Gilbert algorithm. [See Fig. 1.]

Simplifying Eq. (39) by evaluating the trivial ω integral and using the Poisson summation formula to rewrite the sum over $\mathbf{k}$, we reach

$$\begin{aligned}\widehat{\rho}_{\text{free}}(\omega, L, \Delta) - \lim_{L\to\infty} \widehat{\rho}_{\text{free}}(\omega, L, \Delta) &= \sum_{\mathbf{m}\neq\mathbf{0}} \int \frac{d^3\mathbf{k}}{(2\pi)^3} e^{iL\mathbf{m}\cdot\mathbf{k}} \frac{1}{4\omega_{\mathbf{k}}^2} \frac{e^{-(\omega-2\omega_{\mathbf{k}})^2/(2\Delta^2)}}{\sqrt{2\pi}\Delta}\,, \\ &= \frac{1}{(4\pi)^2} \sum_{\mathbf{m}\neq\mathbf{0}} \frac{2\omega}{L|\mathbf{m}|(\omega^2+4M_\pi^2)} \sin\left(\frac{L|\mathbf{m}|}{2\omega}\left(\omega^2-2M_\pi^2\right)\right) \exp\left[\frac{4M_\pi^2}{\Delta^2} - \frac{\Delta^2 L^2 \mathbf{m}^2}{8}\right] + \cdots\,, \end{aligned} \tag{40}$$

where the ellipsis stands for neglected terms suppressed by a power of $\Delta^2 L/\omega$, Δ^2/ω^2 or M_π^2/ω^2.

This result gives a great deal of insight into the deviations between the finite- and infinite-volume spectral functions. As a result of the sin function, the smeared finite-volume spectral function oscillates about its infinite-volume counterpart as ω is varied. Note that, as long as this leading order expression gives a good description, the frequency of oscillation turns out to be independent of the smearing width Δ. We also comment that the exponential factor in Eq. (40) dramatically illustrates the importance of the ordered double limit discussed throughout. In particular, if $\Delta \to 0$ is taken first, then the exponential factor diverges. By contrast, at fixed Δ, the difference between $\widehat{\rho}_{\text{free}}(\omega, L, \Delta)$ and $\lim_{L\to\infty} \widehat{\rho}_{\text{free}}(\omega, L, \Delta)$ vanishes with increasing L as $e^{-\mu^2 L^2}$, with $\mu \equiv \Delta/(2\sqrt{2})$.

We next note that, in the sum over $\mathbf{m}$, a number of terms satisfy $|\mathbf{m}| \in \mathbb{Z}$. This is interesting because these terms vanish identically whenever ω is chosen such that the argument of the sin function becomes an integer multiple of π, i.e. for certain "magic" values satisfying

$$\omega_n = \frac{n\pi + \sqrt{n^2\pi^2 + 2(M_\pi L)^2}}{L}\,, \tag{41}$$

for any integer n. In Fig. 3 we show the result of evaluating the smeared finite-volume spectral function as these special values, as compared to a set of generic values.

To close this subsection we stress that, while this non-interacting example gives a great deal of insight into the finite-volume effects of smeared spectral functions, the quantitative behavior will be

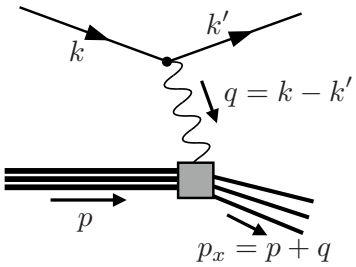

Figure 4. A lepton carrying momentum k scatters off a nucleon with momentum p via exchange of a virtual, space-like photon with momentum q.

significantly modified for a realistic system with particle interactions and with true Backus-Gilbert resolution functions. Extension of these arguments to a realistic application, perhaps making use of the Lellouch-Lüscher technology, is underway.

6 Example application: deep-inelastic scattering

In this section we discuss deep-inelastic scattering (DIS) as a possible application of our Backus-Gilbert spectral-function approach. Other applications are discussed in the publication, Ref. [1].

In order to study the onset of deep-inelastic scattering, and to understand how deviations turn on as one leaves the DIS regime, one must calculate the hadronic tensor, defined by

$$W_{\mu\nu}(p,q) = \frac{1}{4\pi\, n_\lambda} \sum_\lambda \int d^4x\, e^{iq\cdot x} \langle N, \mathbf{p}, \lambda | j_\mu(x) j_\nu(0) | N, \mathbf{p}, \lambda \rangle \,. \tag{42}$$

Here q^μ is the spacelike 4-momentum of the virtual photon ejected by the incident lepton and p^μ the on-shell 4-momentum of the incoming nucleon. [See Fig. 4.] In this work we restrict attention to the unpolarized hadronic tensor.

This hadronic tensor satisfies a simple decomposition into the scalar functions F_1 and F_2, called structure functions

$$W_{\mu\nu}(p,q) = F_1(\nu,x)\left(-g_{\mu\nu} + \frac{q_\mu q_\nu}{q^2}\right) + \frac{F_2(\nu,x)}{p\cdot q}\left(p_\mu - \frac{p\cdot q\, q_\mu}{q^2}\right)\left(p_\nu - \frac{p\cdot q\, q_\nu}{q^2}\right). \tag{43}$$

Note that the structure functions depend on the two available Lorentz scalars, commonly expressed as

$$\nu \equiv \frac{q\cdot p}{M}\,, \qquad x \equiv -\frac{q^2}{2M\nu} \equiv \frac{Q^2}{2M\nu}\,. \tag{44}$$

This assumes the convention that $q^2 < 0$ for spacelike q^μ, i.e. $x > 0$ for physical kinematics. More generally, this discussion is based on Ref. [43] and all conventions and notation are taken from that work.

We have repeated these aspects of standard DIS kinematics because it allows us to describe how the finite resolution of the Backus-Gilbert inversion affects the extraction of $F_1(\nu,x)$ and $F_2(\nu,x)$. In particular, while p^μ and $\mathbf{q}$ are sharply defined in our set up, all extracted quantities are smeared in the remaining coordinate $q^0 \equiv p^0 - p^0_x$. More precisely it is p^0_x, the energy of the outgoing multi-hadron state, that plays the role of ω in Eq. (12).

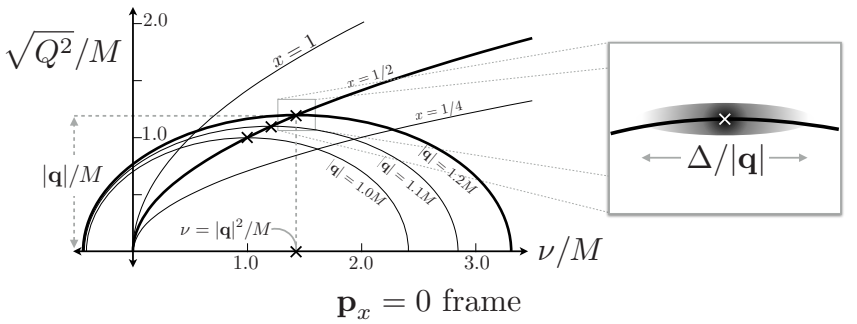

Figure 5. Contours of constant 3-momentum (ellipses) and constant x (square-root functions) in the ν, $\sqrt{Q^2}$ plane. The smearing limits resolution in the direction tangent to the ellipses, as shown in the right panel. The direction perpendicular to the ellipses remains sharp.

Now consider two possible projections of the hadronic tensor. The first option gives direct access to the structure functions

$$F_1(x,\nu) = \frac{1}{2}\Big[- W^{\mu}{}_{\mu}(p,q) + \frac{1}{s_{pq}}\, p^{\mu}p^{\nu}W_{\mu\nu}(p,q)\Big], \tag{45}$$

$$F_2(x,\nu) = \frac{p\cdot q}{2s_{pq}}\Big[- W^{\mu}{}_{\mu}(p,q) + \frac{3}{s_{pq}}\, p^{\mu}p^{\nu}W_{\mu\nu}(p,q)\Big], \tag{46}$$

where $s_{pq} = M^2 - (p\cdot q)^2/q^2$. The second option picks out alternative combinations

$$-s_{pq}F_1(x,\nu) + \frac{s_{pq}^2}{p\cdot q}F_2(x,\nu) = p^{\mu}p^{\nu}W_{\mu\nu}(p,q)\,, \tag{47}$$

$$-3F_1(x,\nu) + \frac{s_{pq}}{p\cdot q}F_2(x,\nu) = W^{\mu}{}_{\mu}(p,q)\,. \tag{48}$$

In fact, these linear combinations are more primary quantities from the perspective of our Backus-Gilbert approach because the projections commute with the inversion. Thus one can apply the second set of projections at the level of the correlation function before using Backus-Gilbert. By contrast, Eqs. (45) and (46) would not be well defined at the level of the correlator, since s_{pq} depends on the inversion coordinate, p_x^0.

Next observe that, although the structure functions depend on only two Lorentz invariants, the lattice calculation is characterized by a total of four degrees of freedom, $\mathbf{p}^2$, $\mathbf{q}^2$, $\mathbf{p}\cdot\mathbf{q}$, p_x^0. The additional degrees of freedom arise because the lattice calculation only has three-dimensional, cubic rotational symmetry, rather than the full Lorentz invariance of the infinite-volume. In principle one can identify different sets of $\{\mathbf{p}^2,\ \mathbf{q}^2,\ \mathbf{p}\cdot\mathbf{q},\ p_x^0\}$ that correspond to the same values of $\{x,\ \nu\}$. By varying the lattice variables over a set that holds x and ν fixed, one gains an additional handle to study the effects of finite-volume and smearing in the extracted structure functions.

In more detail, the relation between the four lattice variables and the relativistic invariants is

$$M\nu = E_{\mathbf{p}}p_x^0 - E_{\mathbf{p}}^2 - \mathbf{q}\cdot\mathbf{p}\,, \tag{49}$$

$$Q^2 = \mathbf{q}^2 - (p_x^0 - E_{\mathbf{p}})^2\,. \tag{50}$$

Eliminating the smeared variable, p_x^0, from Eqs. (49) and (50), we find

$$1 = \frac{Q^2}{\mathbf{q}^2} + \frac{M^2}{E_{\mathbf{p}}^2 \mathbf{q}^2}\left(\nu + \frac{\mathbf{q}\cdot\mathbf{p}}{M}\right)^2 . \tag{51}$$

In words, values of fixed 3-momentum define ellipses in the $(\nu, \sqrt{Q^2})$ plane, and thus the ellipse associated with particular kinematics is certain, but the position along the ellipse is smeared with the resolution function. This is illustrated Fig. 5.

7 Conclusions

In this work we have introduced a new method for directly determining hadronic decay widths and transition rates from lattice data. The central advantage of our approach is that it can accommodate final states with any number of hadrons.

Our idea is to construct a Euclidean correlator such that the corresponding spectral function directly gives the decay width or transition rate of interest. We then advocate using the Backus-Gilbert method, which provides an estimator of the finite-volume spectral function, smeared by a known resolution function $\widehat{\delta}_\Delta(\overline{\omega}, \omega)$ of width Δ. Taking the limit $L \to \infty$ followed by $\Delta \to 0$ then yields the experimental observable. As is illustrated in Fig. 2, a toy study indicates that the finite-volume smeared spectral function can provide a reasonable estimate of its infinite-volume counterpart.

The central advantage of the Backus-Gilbert approach is that it offers a model-independent, unbiased estimator of the smeared, finite-volume spectral function with a precisely known resolution function that is independent of the correlator data. Nonetheless, it may often be the case that the difficulty of reducing the width Δ is the limiting factor of the calculation. To this end we emphasize that one may also smear experimental or model data with the same resolution function to perform a fully controlled comparison. In Sec. 5 we have discussed possible extensions of the basic Backus-Gilbert algorithm that may further improve the quality of extracted data. Ultimately a numerical LQCD calculation is required to fully test the utility of these ideas.

References

[1] M.T. Hansen, H.B. Meyer, D. Robaina (2017), 1704.08993
[2] M. Lüscher, Comm. Math. Phys. **104**, 177 (1986)
[3] M. Lüscher, Nucl. Phys. B **354**, 531 (1991)
[4] M. Lüscher, Comm. Math. Phys. **105**, 153 (1986)
[5] L. Lellouch, M. Lüscher, Comm. Math. Phys. **219**, 31 (2001), hep-lat/0003023
[6] K. Rummukainen, S. Gottlieb, Nucl. Phys. B **450**, 397 (1995), hep-lat/9503028
[7] C. h Kim, C.T. Sachrajda, S.R. Sharpe, Nucl. Phys. B **727**, 218 (2005), hep-lat/0507006
[8] N.H. Christ, C. Kim, T. Yamazaki, Phys. Rev. D **72**, 114506 (2005), hep-lat/0507009
[9] S. He, X. Feng, C. Liu, JHEP **07**, 011 (2005), hep-lat/0504019
[10] M. Lage, U.G. Meißner, A. Rusetsky, Phys. Lett. B **681**, 439 (2009), 0905.0069
[11] V. Bernard, M. Lage, U.G. Meißner, A. Rusetsky, JHEP **2011** (2011), 1010.6018
[12] M. Döring, U.G. Meißner, E. Oset, A. Rusetsky, Eur. Phys. Journal A **47**, 11139 (2011), 1107.3988
[13] Z. Fu, Phys. Rev. D **85**, 014506 (2012), 1110.0319
[14] L. Leskovec, S. Prelovsek, Phys. Rev. **D85**, 114507 (2012), 1202.2145

[15] M. Göckeler, R. Horsley, M. Lage, U.G. Meissner, P.E.L. Rakow, A. Rusetsky, G. Schierholz, J.M. Zanotti, Phys. Rev. D **86**, 094513 (2012), 1206.4141
[16] M.T. Hansen, S.R. Sharpe, Phys. Rev. D **86**, 016007 (2012), 1204.0826
[17] R.A. Briceño, Z. Davoudi, Phys. Rev. D **88**, 094507 (2013), 1204.1110
[18] R.A. Briceño, Phys. Rev. D **89**, 074507 (2014), 1401.3312
[19] M.T. Hansen, S.R. Sharpe, Phys. Rev. D **90**, 116003 (2014), 1408.5933
[20] M.T. Hansen, S.R. Sharpe, Phys. Rev. D **92**, 114509 (2015), 1504.04248
[21] R.A. Briceño, M.T. Hansen, S.R. Sharpe, arXiv:1701.07465, (2017)
[22] H.W. Hammer, J.Y. Pang, A. Rusetsky (2017), 1707.02176
[23] H.B. Meyer, Phys. Rev. Lett. **107**, 072002 (2011), 1105.1892
[24] V. Bernard, D. Hoja, U.G. Meißner, A. Rusetsky, JHEP **09**, 023 (2012), 1205.4642
[25] A. Agadjanov, V. Bernard, U.G. Meißner, A. Rusetsky, Nucl. Phys. **B886**, 1199 (2014), 1405.3476
[26] R.A. Briceño, M.T. Hansen, A. Walker-Loud, Phys. Rev. D **91**, 034501 (2015), 1406.5965
[27] R.A. Briceño, M.T. Hansen, Phys. Rev. D **92**, 074509 (2015), 1502.04314
[28] R.A. Briceño, M.T. Hansen, Phys. Rev. D **94**, 013008 (2016), 1509.08507
[29] N.H. Christ, X. Feng, G. Martinelli, C.T. Sachrajda, Phys. Rev. **D91**, 114510 (2015), 1504.01170
[30] K.F. Liu, S.J. Dong, Phys. Rev. Lett. **72**, 1790 (1994), hep-ph/9306299
[31] U. Aglietti, M. Ciuchini, G. Corbo, E. Franco, G. Martinelli, L. Silvestrini, Phys. Lett. **B432**, 411 (1998), hep-ph/9804416
[32] N.H. Christ, X. Feng, A. Portelli, C.T. Sachrajda (RBC, UKQCD), Phys. Rev. **D92**, 094512 (2015), 1507.03094
[33] N.H. Christ, X. Feng, A. Portelli, C.T. Sachrajda (RBC, UKQCD), Phys. Rev. **D93**, 114517 (2016), 1605.04442
[34] D. Agadjanov, M. Döring, M. Mai, U.G. Meißner, A. Rusetsky, JHEP **06**, 043 (2016), 1603.07205
[35] K.F. Liu, PoS **LATTICE2015**, 115 (2016), 1603.07352
[36] K.F. Liu (2017), 1703.04690
[37] S. Hashimoto (2017), 1703.01881
[38] G. Backus, F. Gilbert, Geophysical Journal of the Royal Astronomical Society **16**, 169 (1968)
[39] G. Backus, F. Gilbert, Philosophical Transactions of the Royal Society of London A: Mathematical, Physical and Engineering Sciences **266**, 123 (1970)
[40] W.H. Press, S.A. Teukolsky, W.T. Vetterling, B.P. Flannery, Cambridge University Press, UK (2007)
[41] B.B. Brandt, A. Francis, H.B. Meyer, D. Robaina, Phys. Rev. **D92**, 094510 (2015), 1506.05732
[42] H.B. Meyer, Eur.Phys.J. **A47**, 86 (2011), 1104.3708
[43] A.V. Manohar, hep-ph/9204208, (1992)